DOMAIN INSTABILITIES IN LIQUID CRYSTALS

L. Blinov

ELECTRICAL EFFECTS AND PHYSICAL APPLICATIONS.

DOMAIN INSTABILITIES IN LIQUID CRYSTALS

L. M. BLINOV

Organic Intermediates and Dyes Institute, K-1, Moscou, U.S.S.R.

Résumé. — On a donné une classification d'instabilités obtenues lorsque des couches nématiques, cholestériques ou smectiques sont placées dans un champ électrique ou magnétique. Le type du couple qui déstabilise la distribution des axes moléculaires (du directeur **L**) est pris pour base de la classification. On a montré, que pratiquement toutes les structures spatiales périodiques observables (domaines) ne peuvent être expliquées qu'à partir de trois couples déstabilisants : diélectrique, flexoélectrique et électrohydrodynamique.

Abstract. — A classification was given of the instabilities appearing in nematic, cholesteric, and smectic liquid crystals exposed to an electric or magnetic field. The basis of the classification is a type of the torque which destabilizes the distribution of molecular axes (director **L**). It was shown that the explanation of practically all the observed spatial periodic patterns (domains) can be given taking only three torques into account : the dielectric, flexoelectric and electrohydrodynamic.

1. **Introduction.** — First of all, liquid crystals are liquids, and all the phenomena which appear in ordinary liquids exposed to an external field take place in liquid crystals as well. The optical effects are very much pronounced in this case because of large optical anisotropy of mesophases. In particular, liquid crystals easily visualize the mass transfer (flow), which is assisted by the director reorientation. Besides, there are some other possibilities to destabilize the uniform initial molecular orientation of a liquid crystal thanks to the anisotropy of the dielectric permittivity or electrical conductivity as well as to some specific collective effects (e.g., the flexo-electric one) [1]. For instance, using an external field one can change the director orientation in pure static way, i.d., without any mass transfer. Such a situation is realized for the Frederiks transition which is due to a pure torsional distortion. The period of the distortion is infinite when boundary conditions are not taken into account.

Electro-optical effects caused by such deformations (e.g., the twist-effect) now have led to the development of various devices and extensive literature has been devoted to this subject [1]. Here, we are interested only in spatially-periodic, field-induced distortions (domains). In our opinion, their technical application is a matter of the nearest future. Up to now there was observed a variety of different domain patterns. If we shall limit ourselves only by those of domains which show up directly from the initial unperturbed state, then the most typical patterns are the following :

a) The transverse (with respect to the director) Kapustin-Williams domains [2, 3] which are excited by a low-frequency field in homogeneously oriented conductive ($\sigma \neq 0$) layers of nematic liquid crystals (NLCs) with negative or slight positive anisotropy of dielectric permittivity, $\varepsilon_a = \varepsilon_{\parallel} - \varepsilon_{\perp}$ (the indices $\parallel$ and $\perp$ refer to the director).

b) The longitudinal domains with a period dependent on strength of d.c. field which are observed in thin homogeneously oriented layers of NLCs at low electrical conductivity ($\sigma \approx 0$) when the transverse domain mode is suppressed [4, 5].

c) The transverse domains and chevrons which appear in homogeneously oriented NLCs at rather high frequencies [6, 7].

d) The domains in the form of Maltese crosses [8, 9] or fingerprints [9, 10] which were observed for homeotropically oriented NLC layers with $\varepsilon_a > 0$.

e) The instabilities in the form of a grid, which are observed for the planar textures of cholesteric liquid crystal (CLCs) at $\sigma \approx 0$ and $\varepsilon_a > 0$ [11] as well as at $\sigma \neq 0$ and $\varepsilon_a < 0$ [12].

f) The transverse and concentric domains which were observed by Goscianski *et al.* [13] respectively in the homogeneously ($\varepsilon_a > 0$) and homeotropically ($\varepsilon_a < 0$) oriented layers of smectic liquid crystals (SLCa) of the type A.

A number of domain patterns listed above generates a need for some systematization of the observed instabilities. The reason producing an instability

TABLE I

Domain instabilities in liquid crystals

Mechanism for director destabilization	Electrical conductivity	Characteristic time for threshold-frequency curve	Characteristic conditions for appearance	Examples	Theory and experiment
Dielectric $M_{diel} \sim \varepsilon_a E^2$	$\sigma = 0$	Debye dipolar relaxation time, τ_D	Lamellar structures of CLCs and SLCs $\varepsilon_a > 0$, homogen. orient	Grid instability in CLCs	Helfrich, 1970 Gerritsma, 1971
				Parodi instability in smectics A	Parodi, 1972 Goscianski, 1975
			$\varepsilon_a < 0$, homeotr. orient.	Undulation instability in SLCs	De Gennes, 1974
Flexo-electric $M_{flex} \sim e^* E$	$\sigma = 0$	Relaxation time for director, T_d	Homogeneously oriented NLCs, d.c. voltage and infra-low freqs. $\lvert \varepsilon_a \rvert < \varepsilon_a^{crit}$	1-dimensional transverse distortions at weak anchorage	Meyer, 1969
				2-dimensional longitudinal distortions in uniform d.c. field	Bobulev and Pikin, 1977 Vistin, 1970 Barnik *et al.*, 1977
				1-dimensional longitudinal distortions in field gradient	Petrov *et al.*, 1974
Electrohydro-dynamic $M_{hydro} \sim \alpha_1 \frac{\partial v_x}{\partial x_l}$ that is, $M_{hydro} \sim \alpha_1 E^2$	$\sigma \neq 0$	Space charge relaxation time, τ_q	1. NLCs, CLCs, SLCs in field gradient σ_a-arbitrary (no injection)	Chevrons (homogen. orient) Maltese crosses, fingerprints (homeotr. orient)	Pikin, 1976 Barnik *et al.*, 1976
		τ_e, when $\tau_e \gg \tau_q$	2. Injection from electrodes σ_a-arbitrary	Irregular 1-dimensional and 2-dimensional patterns	Felici, 1969 Orsay group, 1970
				Transverse Kapustin-Williams domains (homogen. orient.)	Helfrich, 1969 Kapustin *et al.*, 1961 Williams, 1963
		τ_q^*	3. NLCs in uniform field, $\sigma_a > 0$	Fine lattice (homeotr. orient)	Barnik *et al.*, 1975
				Longitudinal domains (tilted orient.)	Pikin, 1976 Ryschenkow *et al.*, 1976

could be a very convenient criterion for the systematization. We have chosen the mechanism of the director destabilization by an electric field as such a criterion. The consideration of only the electric effects does not lead to a lack of generality of the problem as all the magnetic effects in liquid crystals have their electric analogies (the inverse is not true because a number of effects is due to the electric current). Let us discuss separately each of the possible mechanisms of the director destabilization (see table I).

2. **Instabilities caused by the dielectric destabilization.** — Let us consider the simplest case when the electrical conductivity is not essential ($\sigma = 0$) and the molecular dipoles play only indirect role, i.d. determine the value and sign of dielectric anisotropy (the flexo-electric effect is absent). Then, the steady-state distribution of the director ($\mathbf{L}(r)$) can be derived from the condition of minimum free energy which involves the elastic and dielectric (or magnetic) terms. For a volume unit :

$$F = F_{elast} + F_{diel} = F_{elast} + \frac{\varepsilon_a}{8\pi} (\mathbf{E}.\mathbf{L})^2 . \quad (1)$$

In the case of the nematic phase such a minimization does not lead to spatially-periodic solutions but results in the distortion of infinite period (Frederiks transition). For a one-dimensional problem (Fig. 1*a*, *b*) the minimum condition, $F = F_{min}$, can be satisfied by the following Euler equation, which describes the balance of the corresponding torques :

$$M_{elast} + M_{diel} = K_{ii} \frac{\partial^2 \Theta}{\partial z^2} + \frac{\varepsilon_a E^2}{4\pi} \sin \Theta . \cos \Theta = 0 . \quad (2)$$

Here Θ is an angle of the director deviation in the plane xz, $E = E_z$, $K_{ii} = K_{11}$ (Fig. 1*a*) or K_{33} (Fig. 1*b*).

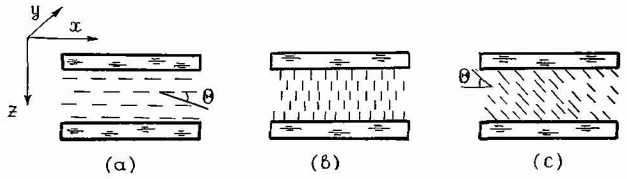

FIG. 1. — The homogeneous (*a*), homeotropic (*b*) and tilted (*c*) orientations of NLCs.

If we deal with lamellar phases the expression for the elastic torque in eq. (1) should be changed. For both cholesteric and smectic A liquid crystals the free energy minimum condition is satisfied by periodic solutions and appropriate domain patterns are observed in experiments.

Figure 2 shows the domain structure in the form of square grid, appearing at a certain threshold voltage in the planar cholesteric texture with $\varepsilon_a > 0$ [11, 14]. The torque balance condition is fulfilled in this case for the wavy periodic distortion [15],

$$\Theta = \Theta_m \sin\left(\frac{\pi z}{d}\right) \cdot \sin\left(\frac{\pi x}{w}\right), \qquad (3)$$

where Θ is an angle of the director deviation from the layer plane, d and w are the thickness in z-direction and domain period in x-direction, respectively (for a three dimensional approach there has also to appear a periodicity along y-axis). The threshold fields of the steady-state distortion are controlled by dielectric anisotropy,

$$E_{th}^2 = \frac{8\pi^2 \sqrt{6 K_{22} \cdot K_{33}}}{P_0 \, d\varepsilon_a}, \qquad (4)$$

where K_{22}, K_{33} are the moduli of the torsion and bend deformations, P_0 is an equilibrium pitch of the cholesteric helix.

The wavy distortion of the type (3) has to occur also in the homeotropically oriented smectic A phase with $\varepsilon_a > 0$, when the field direction coincides with the layer plane. The value for the threshold field can be calculated exactly in the same way if one will change the pitch P_0 by the characteristic length,

$$\lambda_s = \sqrt{K_{11}/\overline{B}},$$

including the elastic moduli K_{11} and $\overline{B}$ of the smectic A phase. Up to now, such an undulation instability in SLCs was only observed under conditions of its mechanical excitation by the layer dilation.

Another example of the domain pattern caused by the pure dielectric destabilization of a lamellar phase is the Parodi instability in a smectic A liquid crystal. Figure 3 shows a model for such an instability for $\varepsilon_a > 0$ and homeotropic orientation [17] and appropriate domain pattern observed in 4-n-butoxybenzylidene-4'-n-octylaniline [13]. The threshold field of the distortion is also controlled by a value of ε_a :

$$E_{th}^2 = \frac{8\pi f}{|\varepsilon_a| ld}, \qquad (5)$$

where l and f are the distance between smectic layers and dislocation energy, respectively.

The threshold field of these instabilities is independent of frequency up to the dispersion range for ε_a determined by one of the Debye dipolar relaxation times, which is proportional to liquid crystal viscosity, $\tau_D \sim \eta/kT$. It is the most characteristic feature of the dielectric destabilization mechanism that is given in table I. Appropriate experimental curves for the grid distortion in CLCs [18] are shown in figure 4 (the drop of curve (1) at low frequencies should be ignored as caused by a non-zero value of electrical conductivity). At frequencies above τ_D^{-1} the threshold

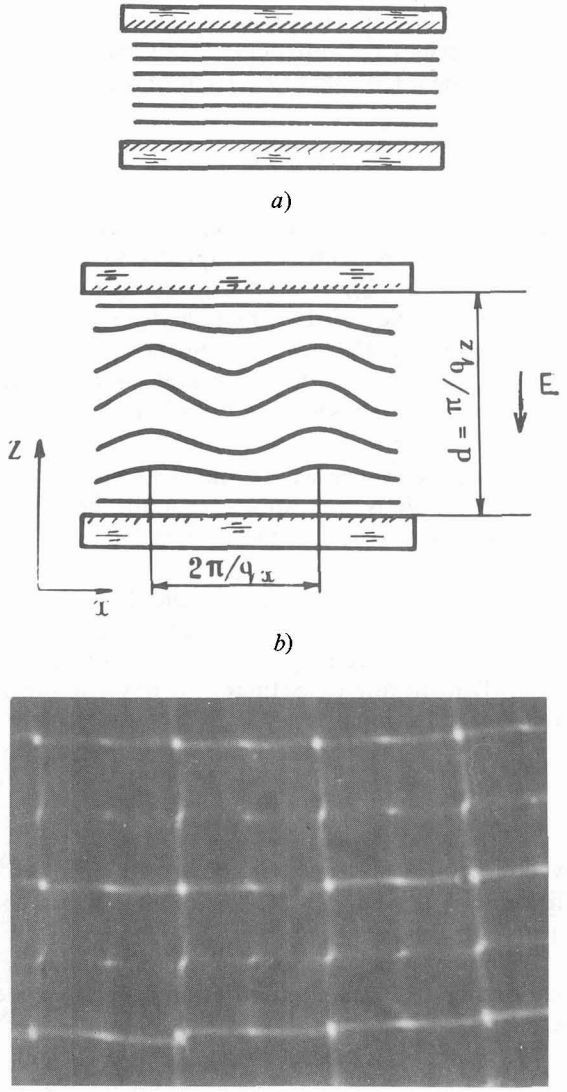

FIG. 2. — The Helfrich dielectric instability in the planar cholesteric texture. *a*) Initial texture ; *b*) Theoretical model for distortion [15] ; *c*) Observed domain pattern (cell dimensions are 80 × 80 μ).

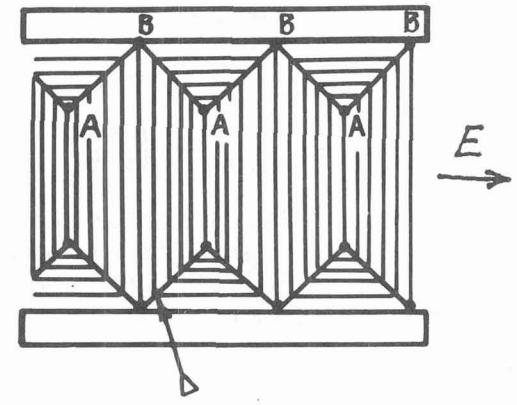

a)

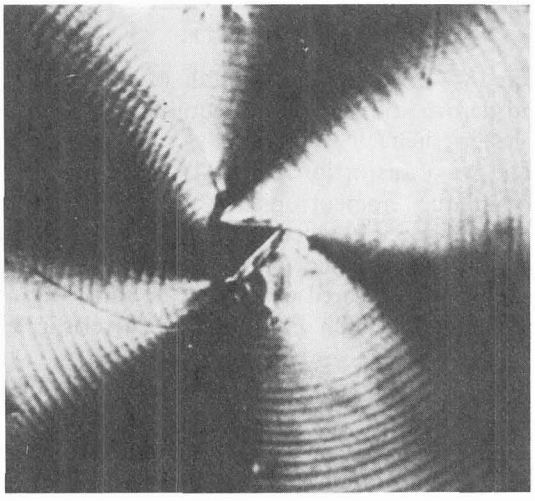

b)

FIG. 3. — The Parodi instability in a smectic A. *a*) Model [17]; *b*) Observed domain pattern [13].

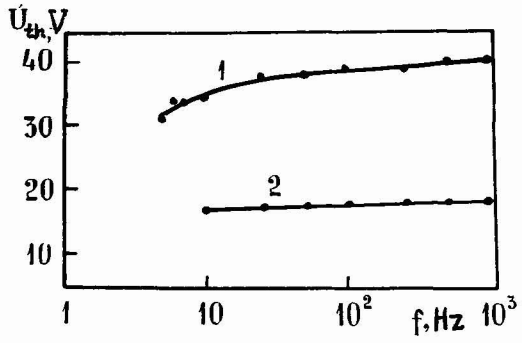

FIG. 4. — Threshold-frequency curves for the Helfrich instability in nemato-cholesteric mixtures [18]; $\varepsilon_a > 0$, $d = 80$ μ, $P_0 = 4$ μ (1), 17 μ (2).

field variations correlate with the frequency changes in ε_a,

$$E_{th}^2(\omega) \sim [\varepsilon_a(\omega)]^{-1} \sim 1 + \omega^2 . \tau_D^2 , \qquad (6)$$

since, in the first approximation, the frequency dependence of moduli K_{ii} may be disregarded (in principle, such a dependence should be borne in mind [19]). To our knowledge, at the present time there are no experimental data on frequency behaviour of the threshold field for dielectrically induced instabilities in the smectic A phase.

As mentioned above, pure dielectric destabilization results in domain patterns only in the case of lamellar mesophases. However, it should be noted that recently Carr has observed domains in NLCs exposed to an magnetic field [20]. This situation is analogous to the dielectric destabilization at $\sigma = 0$. However, the Carr experiments were carried out on rather thick samples and the Frederiks transition was assisted by a noticeable flow of a liquid (the back-flow effect). Thus, the domains arised as a result of the combined effect of the magnetic and hydrodynamic torques and such a situation requires a special consideration.

Strictly speaking, under condition of a non-uniform field the additional term must be involved in eq. (1) which describes the interaction between an external field and the quadrupolar moment of a medium,

$$F_Q = Q \frac{\partial E_i}{\partial x_k} L_i L_k , \qquad (7)$$

where Q is a difference between longitudinal and transverse components of a quadrupolar moment density tensor. This term can change essentially the characteristics of the Frederiks transition caused by the field of a charged solid surface [21]. Whether it can result in periodic structures in the nematic and other mesophases is a question to be solved.

3. **Instabilities caused by the flexo-electric destabilization.** — It is well known that the flexo-electric effect results from the linear coupling between an electric field and liquid crystal distortion [1, 16]. It can be produced by either the dipolar polarization of a medium (under the assumption of a specific form of the molecules) [22] or quadrupolar interaction [23]. In any case, there is a novel term in the free energy formula :

$$F_{flex} = \mathbf{E}\mathbf{P}_{flex} = \mathbf{E}[e_{1z}\,\mathbf{L}(\mathrm{div}\,\mathbf{L}) + e_{3x}(\mathrm{rot}\,\mathbf{L})\times\mathbf{L}] , \qquad (8)$$

where P_{flex} is a flexo-electric polarization in the field direction, e_{1z} and e_{3x} are the flexo-electric coefficients [22].

In the simplest case of a one-dimensional deformation, figure 1*a*, the minimization of the free energy functional,

$$F = F_{elast} + F_{diel} + F_{flex} , \qquad (9)$$

results in the same Euler eq. (2) which is indicative of an absence of any volume flexo-electric torque exerted on the director. However, the torque takes place at the sample boundaries and the deformation

starts from there. As a result, the steady-state domain structure can develop with a period along the x-axis [22],

$$w = \frac{\pi K_{11}}{e_{1z} E}. \tag{10}$$

If the z-dimension of a sample is infinite, the domains (Fig. 5) arise at an infinitesimal field $E = E_z$. The crucial condition for existence of these (transverse) domains is a small value of dielectric anisotropy [24].

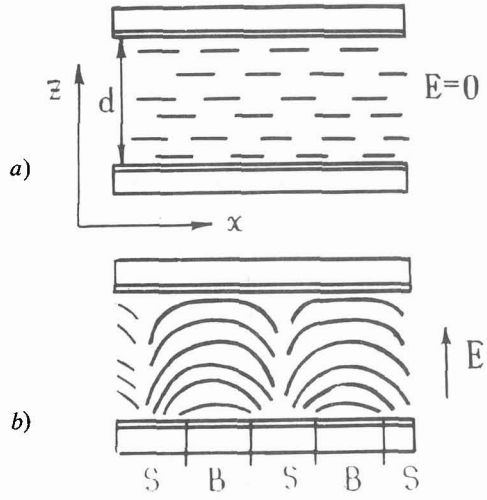

FIG. 5. — The initial NLC orientation (a) and the Meyer model [22] for flexo-electric domains (b).

Up to now, such an instability has not been detected in experiments. Nevertheless, for one-dimensional geometry (Fig. 1b, a field is directed along x) Petrov and Derzhanski [25] observed the waves of the flexo-electric deformation which spread from the sample boundaries into its volume and produced some resonance optical effects. These observations confirm the important role of the surface flexo-electric torques.

Recently [26] Bobylev and Pikin have shown, that the volume flexo-electric torques,

$$M_{\text{flex}} = -\frac{e^* E}{K}\frac{\partial \Theta}{\partial y} \quad \text{or} \quad \frac{e^* E}{K}\frac{\partial \varphi}{\partial y}, \tag{11}$$

exerted on the director in the case of two-dimensional

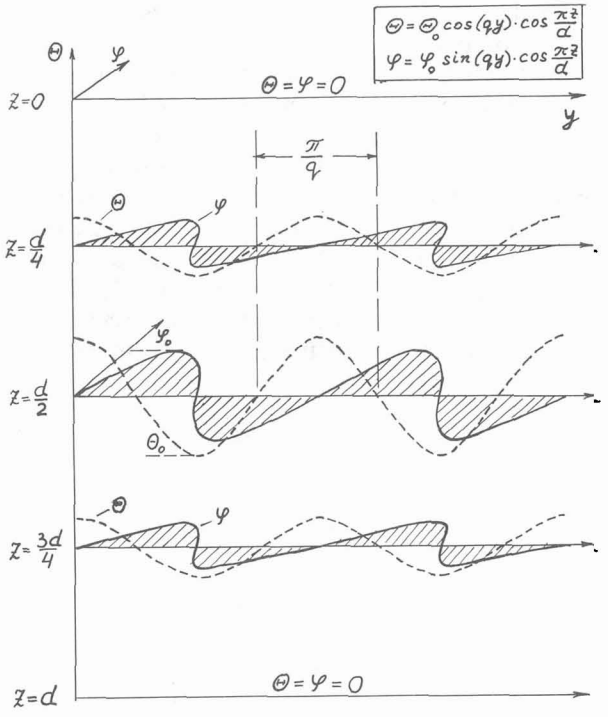

FIG. 6. — Two-dimensional flexo-electric distortion predicted by Bobylev and Pikin [26].

deviations from the same initial state (Fig. 1a), can result in flexo-electric domains of another type (longitudinal domains). In eq. (11) $e^* = e_{1z} - e_{1x}$, $K = K_{ii}$, Θ is a director tilt angle in plane xz, φ is director azimuth in plane xy. The two-dimensional deformation corresponding to the longitudinal domains is shown schematically in figure 6.

The Pikin-Bobylev flexo-electric domains are characterized by a sharp threshold (under condition of strong surface anchorage) and the specific dependences of the threshold field and domain period (at E_{th}) on dielectric anisotropy :

$$E_{\text{th}} = \frac{2\pi K}{|e^*|(1+\mu)d}; \qquad w_{\text{th}} = \frac{d}{\pi}\sqrt{\frac{1+\mu}{1-\mu}}, \tag{12}$$

where $\mu = \varepsilon_a K/4\pi e^{*2}$.

It is the longitudinal domains mentioned in point (b) of Introduction which are caused by the flexo-electric destabilization of a homogeneously oriented NLC

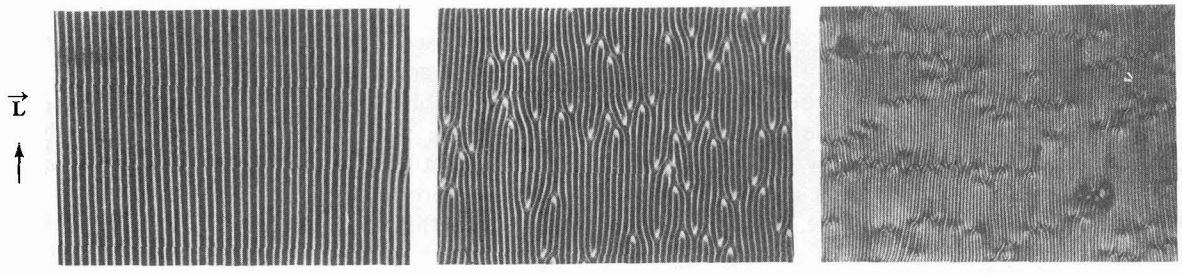

FIG. 7. — Longitudinal flexo-electric domains in p-n-butyl-p'-methoxy-azoxybenzene (BMOAOB) (homogeneous orientation, $d = 12$ μ, $\varepsilon_a = -0.25$, $T = 25$ °C, frame dimensions are 600 × 400 μ). D.C. voltage : 16 V (a), 25 V (b) and 50 V (c).

layer. In order to observe such domains it is of importance to choose a proper value for ε_a and suppress electrohydrodynamic instabilities. The second condition is fulfilled in azoxycompounds and other electrochemically stable NLCs at a d.c. voltage because of the inevitable electrolytic purification of substance. Figure 7 shows microphotographs of the domain pattern observed by Barnik *et al.* [5]. The experimental dependences of E_{th} and w_{th} on dielectric anisotropy (Fig. 8) agree well with expressions (12) (here the dielectric torque stabilizes the initial structure). The critical value for ε_a in the range $\varepsilon_a < 0$ also agrees with the theory :

$$|\varepsilon_a| \leqslant \frac{4\pi e^*}{K}. \tag{13}$$

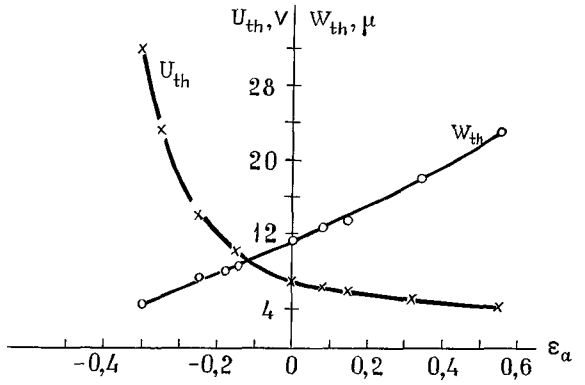

FIG. 8. — The threshold voltage U_{th} and period w_{th} (at U_{th}) for flexo-electric domains *vs* dielectric anisotropy in doped BMOAOB. The divergency of U_{th} at $\varepsilon_a^{crit} \approx -0.56$ is well seen.

In the case of a non-uniform field the volume flexo-electric torque can also arise for the one-dimensional model. Then it is proportional to the field gradient and can result in periodic distortion patterns in the form of domains perpendicular to the initial orientation of the director. There have been published only previous results of the observation of such domains [27].

As the flexo-electric torque (and, consequently, the associated distortion) changes sign at field polarity switching, the director relaxation time manifests itself as a characteristic time for the threshold-frequency curve [26] :

$$T_d \approx \frac{\gamma_1 d^2}{\pi^2 K}. \tag{14}$$

Here γ_1 is the twist-viscosity coefficient. Usually T_d is of the order of 0.1-1 s and the threshold voltage increases sharply even at infra-low frequencies. That is why the flexo-electric domains are hardly observable at an a.c. voltage ; as a rule, they are masked by electrohydrodynamic processes.

The most characteristic features of the flexo-electric instabilities are given in the second line of table I.

4. **Instabilities caused by the electrohydrodynamic (EHD) destabilization.** — If a liquid moves for any reason the kinetic energy term should be involved in the free energy functional [16]. However, we cannot next minimize the functional as the system is not at equilibrium because of dissipative processes. Thus, in this case, it is more convenient to start directly from the equations which couple acting forces with velocity of a fluid.

In liquid crystals, the flow gives rise to the reorientation of the director. The appropriate torque is proportional to velocity gradient

$$M_{hydro} \sim \alpha \nabla \mathbf{v}, \tag{15}$$

where α is a friction coefficient that takes account of the geometry of an experiment.

In liquids of low conductivity the electro-neutrality of the medium can easily be disturbed, i.d., the space charge δq can appear for different reasons. Interacting with an external field, this charge, according to the Navier-Stokes equation, gives rise to movement of a liquid (η is a viscosity) :

$$v \sim \frac{E.\delta q}{\eta}. \tag{16}$$

So, if there is a space charge, a liquid can move, and, if the velocity field is non-uniform, the torque M_{hydro} arises which destabilizes the initial orientation of the director. The reasons responsible for the formation of the space charge can be different (see below) but, as a rule, the value of δq is proportional to the field ; hence, both v and M_{hydro} are proportional to E^2. In this case, the director *feels* the r.m.s. value of an a.c. field and the Maxwell space charge relaxation time determines the frequency behaviour of the threshold field for the instability :

$$\tau_q = \frac{\varepsilon}{4\pi\sigma}. \tag{17}$$

According to mechanisms responsible for the space charge formation we can distinguish three types of EHD instabilities resulting in domain patterns in liquid crystals.

(i) The most general of them seems to be the space charge formation for the electrolytic separation of positive and negative charges by an external field itself, see figure 9*a*. It should be noted that now we do not consider any charge injection ; e.g., electrodes can be blocked with thin dielectric layers and an a.c. voltage applied across them. Near the electrode (at the distance L_D), where the space charge gradient (proportional to vE where v is an electrokinetic coefficient) coincides with the field direction, figure 9*a*, the field produces the destabilizing force $E.\delta q(z)$ just in the same way as a temperature gradient destabilizes the liquid placed in a gravity field (the Benard problem [28]), figure 10*a*. Such an instability

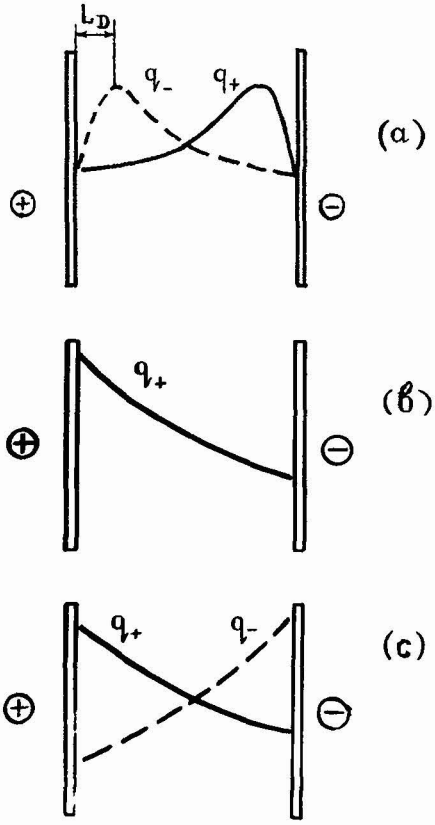

FIG. 9. — Distributions of densities of positive q_+ and negative q_- space charges for : *a*) their electrolytic separation ; *b*) unipolar injection ; *c*) bipolar injection. L_D is the Debye length.

was observed over a wide frequency range for both the isotropic and nematic phases [7, 10] as well as for CLCs [29] and SLCs [30]. Of course, the appearance of domain patterns is dependent on the type

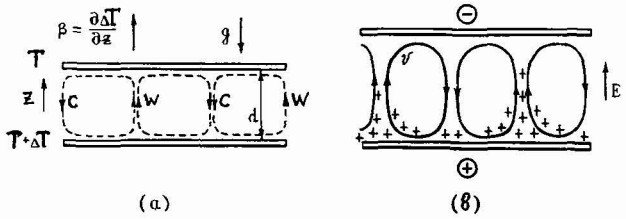

FIG. 10. — *a*) Convective instability caused by the temperature gradient directed from below (cold and warm streams are marked by letters C and W) ; *b*) EHD instability caused by a unipolar charge injection.

of a mesophase and its orientation. Let us consider some examples.

Figure 11 shows the photographs of domains which occur in homeotropically oriented NLC layers at $\varepsilon_a > 0$ and $E = E_z$ when the dielectric torque is

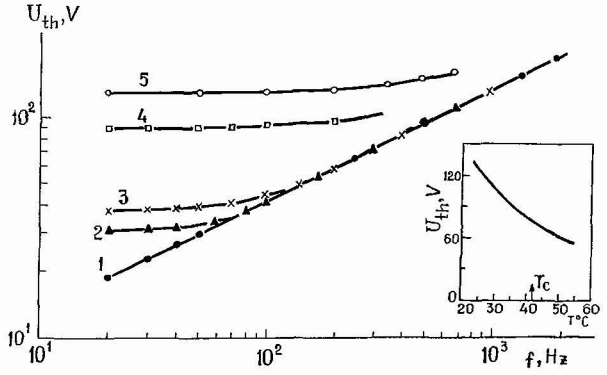

FIG. 12. — The isotropic mode : frequency dependences of domain threshold voltage for homeotropically oriented NLCs with $\varepsilon_a > 0$ (doped MBBA, $T = 22$ °C, $d = 20$ μ) [7]. 1 : $\varepsilon_a = 6.5$; $\sigma_{\parallel} = 4 \times 10^{-11}\ \Omega^{-1}.\text{cm}^{-1}$. 2-5 : $\varepsilon_a = 0.1$; $\sigma_{\parallel} = 4.2 \times 10^{-10}$ (2), 5.6×10^{-10} (3), 2.6×10^{-9} (4), 5.5×10^{-9} (5) $\Omega^{-1}.\text{cm}^{-1}$. Insert : the temperature behaviour of the threshold ; T_c is a clearing point.

FIG. 11. — Fingerprint domains at frequencies $\omega < \tau_q^{-1}$ (*a*) and Maltese crosses at frequencies $\omega > \tau_q^{-1}$ (*b*) for homeotropically oriented NLCs (doped MBBA, $\varepsilon_a > 0$, $d = 20$ μ, $T = 20$ °C) [7].

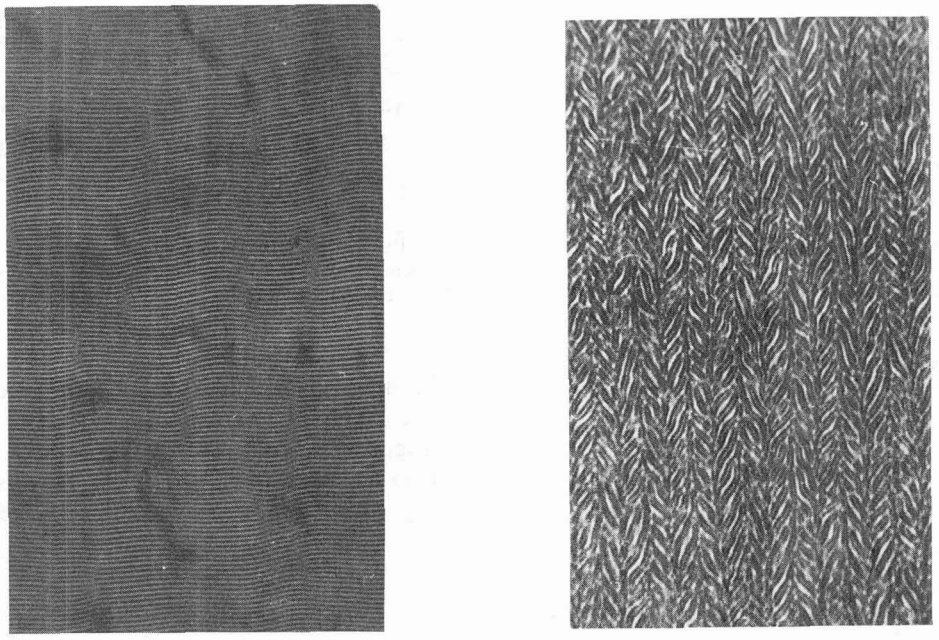

(a) (b)

FIG. 13. — The instability pattern for a homogeneously oriented NLC with $\varepsilon_a < 0$ [7]. *a*) Transverse (pre-chevron) domains at the voltage just above the threshold ; *b*) Chevron structure.

stabilizing and the flexo-electric one is equal to zero. The frequency dependence of the threshold for this instability is given in figure 12. It is very important that the threshold voltage for the circular movement of a liquid which is responsible for the domains does not change just at the phase transition to the isotropic phase, though, of course, the optical pattern disappears (see Insert in figure 12).

The same type of destabilization is also responsible for the lowest voltage instability branch in homogeneously oriented NLC layers with $\varepsilon_a < 0$, figures 13, 14 [6, 7]. As in the case of the homeotropic orientation, the threshold field is determined by isotropic parameters of the substance :

$$E_{th}^2 = \frac{\text{const.}\,\eta\sigma}{\nu.\varepsilon^2} \quad \text{at} \quad \omega \ll \tau_q^{-1}\,, \qquad E_{th}^2 = \frac{\text{const.}\,\eta\omega}{\nu.\varepsilon} \quad \text{at} \quad \omega \gg \tau_q^{-1}\,. \tag{18}$$

At last, the same dependences of E_{th} on ω and material parameters can be demonstrated in the cases of CLCs (Fig. 15), smectics A, and nematic phase with some smectic ordering and $\sigma_a < 0$ (Fig. 16). For instance, one can see in figure 15 that E_{th} is almost independent of the pitch of the cholesteric helix (it is not so in the cases of the dielectric destabilization, see figure 4, and the electrohydrodynamic Helfrich model, see below). Though the domain patterns corresponding to figures 15 and 16 have the specific appearance [29, 30], there is no doubt that they were caused by the same destabilizing mechanism.

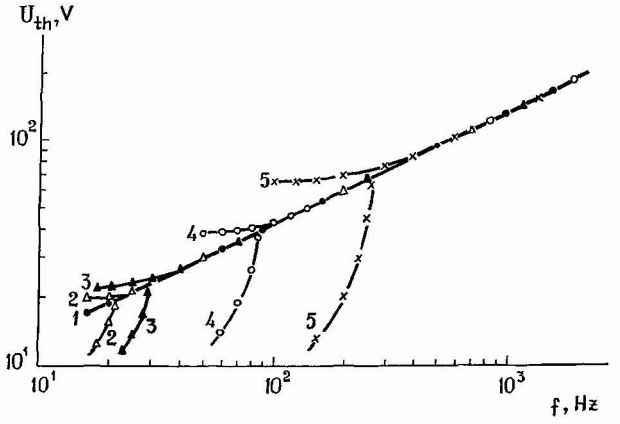

FIG. 14. — The isotropic mode : frequency dependences of pre-chevron domain threshold in NLCs with $\varepsilon_a < 0$ (doped MBBA, $d = 20\,\mu$, 22 °C) [7]. $\sigma_{\parallel} = 3 \times 10^{-11}$ (1), 4×10^{-11} (2), 5.5×10^{-11} (3), 1.5×10^{-10} (4), 5×10^{-5} (5) $\Omega^{-1}.\text{cm}^{-1}$. $\varepsilon_a = -0.1$ (2), -0.5 (1, 3-5).

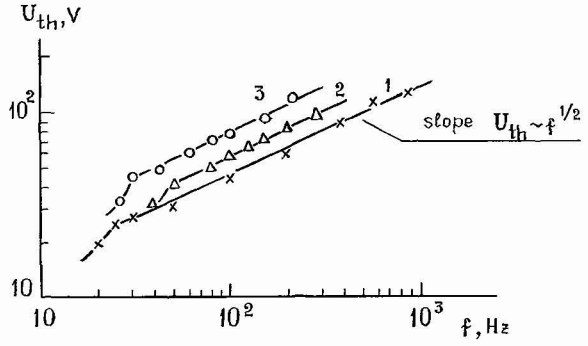

FIG. 15. — The isotropic mode : frequency dependences of the high-frequency instability in nemato-cholesteric mixtures (MBBA doped with a cholesteryl decanoate, 22 °C, $d = 24\,\mu$, the planar texture, $\varepsilon_a < 0$). Pitch of the helix : $P_0 = \infty$ (1), 10 μ (2) and 1 μ (3).

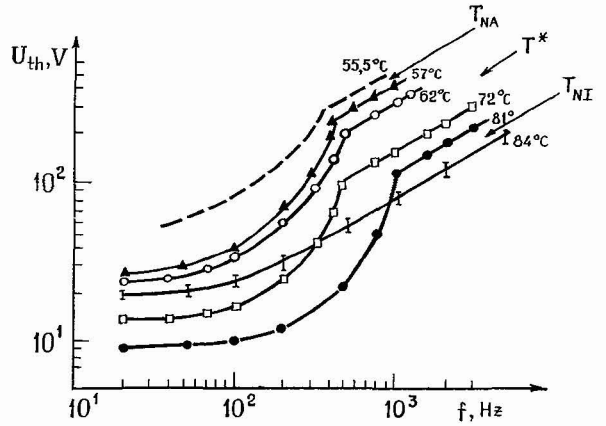

FIG. 16. — The modified isotropic mode : threshold-frequency curves for a domain instability in p-n-butoxy-benzylidene-p'-n-heptylaniline near the phase transition from the nematic phase to a smectic A. Transition temperatures : $T_{NI} = 83.5$ °C, $T_{NA} = 56$ °C, $T^*(\sigma_a = 0) = 67$ °C. The dash curve referred to the smectic phase, was measured with a less accuracy.

(ii) The charge injection from electrodes discussed by Felici [31] can be another reason responsible for the space charge formation. The distribution of δq over the cell thickness is shown in figure 9*b* and *c* for an unipolar and bipolar injection, respectively. Here again, the interaction between the space charge and field gives rise to the vortical movement of a liquid. This movement, figure 10*b*, can be observed in any weakly conductive liquid placed in a d.c. electric field. The threshold voltage for such a hydrodynamic process has the form

$$U_{th} = T \frac{4\pi\eta\,\mu_D}{\varepsilon}, \qquad (19)$$

where μ_D is a drift ion mobility and T is a numerical stability criterion ($T \approx 10^2$) dependent on the intensity of unipolar [32] or bipolar [33] injection.

In liquid crystals, this vortical movement destabilizes the molecular distribution. For example, such a mechanism is responsible for the domain pattern depicted in figure 17, which was observed in MBBA at a d.c. voltage [34].

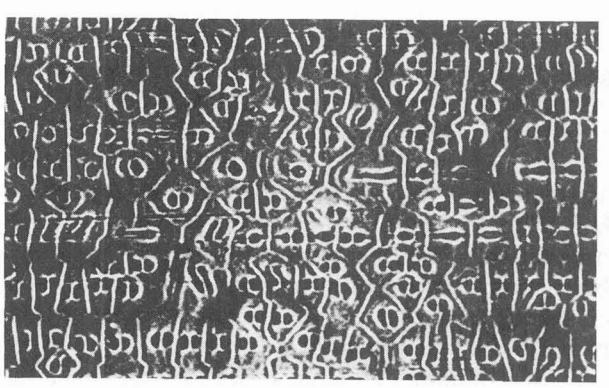

FIG. 17. — Domain pattern in MBBA at a D.C. voltage (U = 7 V) which is due to the charge injection from electrodes [33].

The frequency behaviour of the threshold voltage is determined by the slowest stage of the space charge formation which, in this case, is the electrochemical process at electrodes, $\tau_e \gg \tau_q$. Let us emphasize once more that the mechanisms of the space charge formation discussed in points (i) and (ii) did not caused explicitly by the anisotropy of electrical conductivity though it can modify threshold voltages for domain formation, see below.

(iii) Today, the only ionic mechanism of space charge formation seems to be specific for liquid crystals. This is the Carr-Helfrich mechanism [35] which is due to the conductivity anisotropy

$$(\sigma_a = \sigma_{\parallel} - \sigma_{\perp} \neq 0).$$

Let us consider a homogeneously oriented NLC layer, figure 1*a*, at $\sigma_a > 0$. In this case, the field E_z produces the space charge gradient along the x-axis, $\delta q_x \sim \sigma_a E_z$. For the sake of simplicity, let us assume $\varepsilon_a = 0$. Then, starting from the balance equation for the elastic and hydrodynamic torques,

$$M_{elast} + M_{hydro} = K_{33} \frac{\partial^2 \Theta}{\partial x^2} - \alpha_2 \frac{\partial v_z}{\partial x} = 0, \qquad (20)$$

and taking into account the coupling between the fluid velocity (v_z) and electric field via the Navier-Stokes and Poisson equations, we obtain the spatially-periodic (along x) solutions for v_z, and δq. The x-period of the most energetically favorable distortion is about of π/d because of the cylindrical form of vortices, and the threshold voltage of the instability is :

$$U_{th}^2 = \frac{4\pi^3 K_{33}\,\sigma_{\parallel}\,\eta_1}{(-\alpha_2)\,\varepsilon\sigma_a}. \qquad (21)$$

Here α_2 is the *active* friction coefficient destabilizing the director according to eq. (20), while η_1 is a passive combination of viscosity coefficients which is involved in the Navier-Stokes equation to account for the energy dissipation associated with the field-induced movement of charge δq. For $\varepsilon_a \neq 0$ the dielectric torque must be added in eq. (20) and we arrive to more complex formula for the threshold voltage [35].

In accordance with eq. (21) and experimental data [36], $U_{th} \to \infty$ at $\sigma_a \to 0$. Moreover, the same instability shows up at high frequencies where σ_a increases due to the dielectric losses caused by the dispersion of dielectric permittivity [37]. Thus, there is no doubt that the instability results from the conductivity anisotropy. In experiments it occurs in the form of domains perpendicular to the direction of molecular axes (Kapustin-Williams domains [2, 3]). The observed pattern, the sketch of the NLC vortical movement and corresponding changes in the director inclination from the x-axis are shown in figures 18*a* and 19*a*.

For the initial homeotropic orientation the desta-

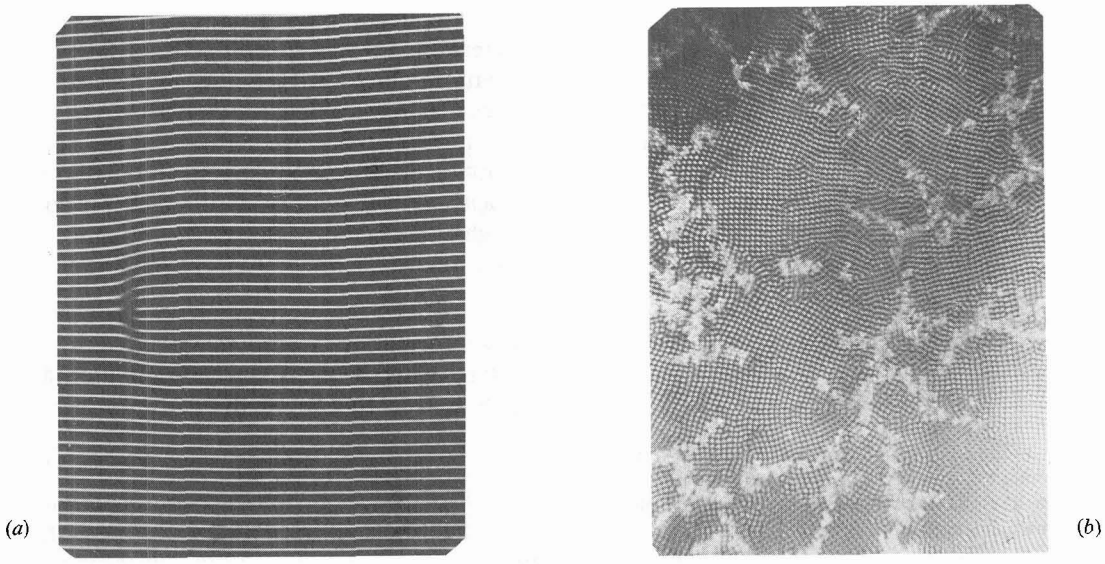

(*a*) (*b*)

FIG. 18. — *a*) Kapustin-Williams domains in a homogeneously oriented layer of MBBA ($U = 7.5$ V, $f = 64$ Hz, domain period is 20 μ). *b*) Instability in the form of fine lattice in a homogeneously oriented layer with $\varepsilon_a \approx 0$ (doped MBBA, $\sigma \approx 10^{-8}\ \Omega^{-1}.\text{cm}^{-1}$, $U = 98$ V, $d = 40$ μ) [38].

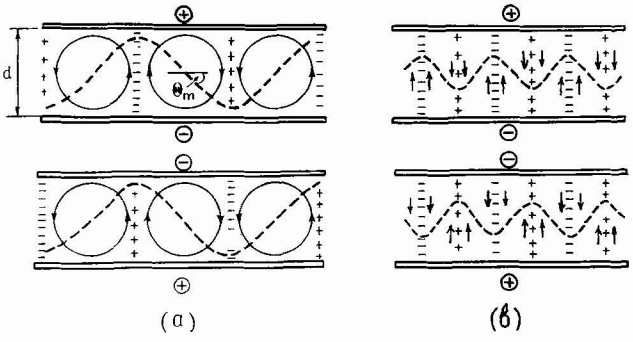

FIG. 19. — Distributions of the space charge and director inclination angle (dash lines) at different field polarities for Kapustin-Williams domains at frequencies below the critical (*a*) and for « dielectric » regime at frequencies above the critical (*b*) : flows are shown by arrows

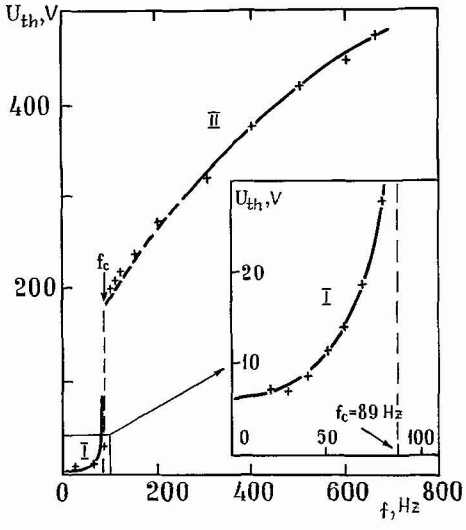

FIG. 20. — The Helfrich EHD instability : threshold-frequency curve for MBBA ($d = 100$ μ, $T = 25$ °C) [6]. Region I : The threshold of Kapustin-Williams domains caused by anisotropic properties of a NLC. Region II : As in the case of figure 14, should be referred to the isotropic mode.

bilizing effect of torque $|\alpha_3\, \partial v_z/\partial x|$ is compensated by stabilizing torque $|\alpha_2\, \partial v_x/\partial z|$ appearing near cell electrodes. As $|\alpha_2| \gg |\alpha_3|$ the instability can occur only under condition that the vortices would be not cylindrical but contracted along the x-direction, that is, the domain pattern has to have a small period compared with the cell thickness. Such a pattern has been observed in [38], figure 18*b*.

The Carr-Helfrich mechanism is also responsible for domains which were observed in homeotropically oriented layers exposed to a field perpendicular to the director [39].

With increasing frequency up to the critical, which now is determined by a new space charge relaxation time τ_q^* involving anisotropic parameters of a liquid crystal, the threshold voltage increases sharply, figure 20, because of the decrease in the amplitude of the space charge separated along x [40]. According to the one-dimensional theory of Orsay group [40, 41], at frequencies above the critical the instability regime has to change significantly. The steady-state distortion shown in figure 19*a* is replaced by periodic oscillations of the director, figure 19*b*. The threshold field of this new (so-called *dielectric*) regime has to depend strongly on anisotropic parameters of a liquid crystal [40, 7]. The latter result has been confirmed recently by extensive numerical calculations which were carried out for the more rigorous two-dimensional model [42].

In our opinion, the true *dielectric* regime of the Carr-Helfrich instability has not been observed yet in experiments because of the masking action of the

isotropic instability discussed above, which has the same frequency dependence of the threshold field, $E_{th} \sim \omega^{1/2}$ ([1]).

At low frequencies and under condition that $\sigma_a > 0$ the Carr-Helfrich instability has been also observed in CLCs and in the nematic phases with some smectic ordering. If the cell thickness is considerably more than the pitch of the helix, the domain pattern takes the same form as in figure 2*b*, *c* [12]. For $d \approx P_0$ one can observe a number of either one-dimensional or two-dimensional periodic distortions in different Grandjean zones, figure 21. In this case, the threshold voltage oscillates with increasing cell thickness, figure 22 [43] (at $d \gg P_0$ this dependence becomes monotonic [44, 45, 14]).

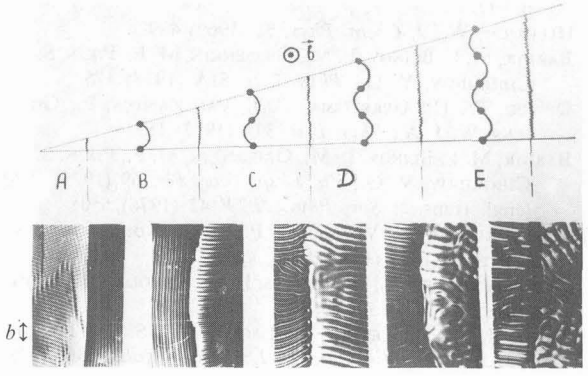

FIG. 21. — Threshold deformation pattern near Cano-Grandjean disclinations in the planar cholesteric texture ($P_0 = 115$ μ). Arrow $\vec{b}$ shows the rubbing direction of glass plates.

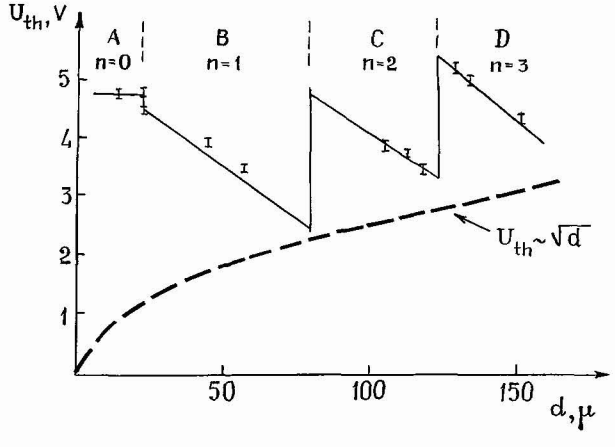

FIG. 22. — Oscillatory dependence of the threshold voltage on the thickness of a planar cell ($P_0 = 115$ μ) [43]. The dash curve is based on the Helfrich-Hurault theory [44] for the case $d \gg P_0$. *n* is the number of half-turns of the helix in the Granjean zone.

([1]) It has been found just before the 7th Int. Conf. on Liquid Crystals by Durand and Ribotta (see abstracts of the conference, post deadline supplement).

Using the Carr-Helfrich model one can explain [46] the formation of longitudinal domains (their direction coincides with the director projection on the layer plane) in the case of the initial tilted orientation, figure 1*c*. The threshold voltage for such an instability is calculated from the balance of the stabilizing elastic torque and destabilizing electrohydrodynamic one caused by conductivity anisotropy [47],

$$U_{th} \sim \frac{K^{1/2}}{\sin \Theta_0}, \qquad (22)$$

where Θ_0 is an initial tilt angle of the molecules.

The longitudinal domains of electrohydrodynamic nature were also observed at $\sigma_a < 0$ in the nematic phases with short-range smectic A ordering [48, 49, 30]. In our opinion, the conductivity anisotropy results in additional space charge which indirectly modifies the frequency dependences of the threshold field for the isotropic instability discussed in point (i). At present, this problem needs be considered theoretically.

5. **Conclusion.** — Thus, we have considered the most typical examples of domain patterns which were mentioned in Introduction. Of course, they do not exhaust a number of observed instabilities. For instance, we do not even touch on little studied instabilities in the smectic C and B phases as well as in the chiral ferroelectric phases C* and H*. In addition, various modes often interfere, resulting in very complex patterns. To illustrate, the combination of the flexo-electric and electrohydrodynamic modes results in oscillatory solutions [50], however, up to now, there are no experimental data on this theme. A list of the domain patterns observed in liquid crystals grows steadily but, unfortunately, not in all the papers one can find enough information to refer one or another phenomenon to a certain mechanism.

Meanwhile, appropriate references are of importance not only from the scientific but from the practical point of view as well. For example, to reduce the threshold field for an instability of homogeneously oriented layers one must increase $|\varepsilon_a|$ in the case of the dielectric destabilization and decrease $|\varepsilon_a|$ when the instability is caused by the flexo-electric or electrohydrodynamic torques. Just so, different parameters are responsible for the spatial period, frequency spectrum and kinetics of various instabilities.

The author is grateful to S. A. Pikin and V. G. Chigrinov for many helpful discussions, and M. I. Barnik, S. V. Belyayev and A. N. Trufanov for supplying their experimental results.

References

[1] BLINOV, L. M., *Elektro-i magnitooptika zhidkikh kristallov* The Electro- and Magneto-Optics of Liquid Crystals (Nauka Publ., Moscow) 1978 (in Russ.).

[2] ZVEREVA, G. E., KAPUSTIN, A. P., In book : *Primenenie ultra-akustiki k issledovaniyu veshchestva* (The application of ultra-acoustics to the investigation of matter), issue 15, Moscow, 1961, p. 69 (in Russ.).

[3] WILLIAMS, R., *J. Chem. Phys.* **39** (1963) 384.

[4] VISTIN', L. K., *Kristallografya* **15** (1970) 594. *Dokl. Akad Nauk SSSR* **194** (1970) 1318.

[5] BARNIK, M. I., BLINOV, L. M., TRUFANOV, A. N., UMANSKI, B. A., *Zh. Eksp. Teor. Fiz.* **73** (1977) 1936 ; *J. Physique* **39** (1978) 417.

[6] ORSAY LIQ. CRYST. GROUP., *Phys. Rev. Lett.* **25** (1970) 1642.

[7] BARNIK, M. I., BLINOV, L. M., GREBENKIN, M. F., TRUFANOV, A. N., *Mol. Cryst. Liq. Cryst.* **37** (1976) 47.

[8] KIRSANOV, E. A., *Uchen. Zapiski. IvGU* (Proc. of Ivanovo State Univ.) **128** (1974) 58.

[9] BARNIK, M. I., BLINOV, L. M., PIKIN, S. A., TRUFANOV, A. N., *Zh. Eksp. Teor. Fiz.* **72** (1977) 756 (Engl. transl. : *Sov. Phys. JETP* **45** (1978) 396).

[10] KASHNOW, R. A., COLE, H. S., *Mol. Cryst. Liq. Cryst.* **23** (1973) 329.

[11] GERRITSMA, C. J., P. VAN ZANTEN, *Phys. Lett.* **37A** (1971) 47.

[12] RONDELEZ, F., ARNOULD, H., *C. R. Hebd. Séan. Acad. Sci.* **273B** (1971) 549.

[13] GOSCIANSKI, M., LEGER, L., MIRCEA-ROUSSEL, A., *J. Physique Lett.* **36** (1975) L-313.

[14] RONDELEZ, F., HULIN, J., *Solid State Commun.* **10** (1972) 1009.

[15] HELFRICH, W., *Appl. Phys. Lett.* **17** (1970) 531.

[16] DE GENNES, P. G., *The Physics of Liquid Crystals* (Clarendon Press, Oxford) 1974.

[17] PARODI, O., *Solid State Commun.* **11** (1972) 1503.

[18] RONDELEZ, F., ARNOULD, H., GERRITSMA, C., *Phys. Rev. Lett.* **28** (1972) 735.

[19] GRULER, H., *J. Chem. Phys.* **62** (1974) 5408.

[20] CARR, E. F., *Mol. Cryst. Liq. Cryst.* (Letters) **34** (1977) 159.

[21] TIKHOMIROVA, N. A., PIKIN, S. A. *et al.*, *Kristallografiya* **23** (1978) 1239.

[22] MEYER, R. B., *Phys. Rev. Lett.* **22** (1969) 918.

[23] PROST, J., MARCEROU, J. P., *J. Physique* **38** (1977) 315.

[24] DMITRIYEV, S. G., *Zh. Eksp. Teor. Fiz.* **61** (1971) 2049 ; FAN, C., *Mol. Cryst. Liq. Cryst.* **13** (1971) 9.

[25] DERZHANSKI, A., PETROV, A. C., *1 Flussigkrist. Konf. soz. Länder, Halle*, DDR, 1976. Kurzref. s. 78.

[26] BOBYLEV, Ju. P., PIKIN, S. A., *Zh. Eksp. Teor. Fiz.* **72** (1977) 369.

[27] PETROV, A. G., Ph. D. Thesis, Sofia, Bulgaria (1974) ; Liq. Cryst. Abstr. 00028. Derzhanski, A., Plenary Lect. at Conversatorium on Liq. Cryst., Rzeszow, Poland, 1975.

[28] GUYON, E., PIERANSKI, P., *Physica* **73** (1974) 184.

[29] BELYAYEV, S. V., KARAZHAYEV, V. D., TRUFANOV, A. N., *IV All-Union Conf. on Liquid Crystals* (Ivanovo) 1977. Abstracts, p. 75.
BELYAEV, S. V., *Zh. Eksp. Teor. Fiz.* **75** (1978) 705.

[30] BARNIK, M. I., BLINOV, L. M., LAZAREVA, V. T., TRUFANOV, A. N., *VII Int. Conf. on Liq. Cryst. Bordeaux*, France, 1978. Abstracts.

[31] FELICI, N., *Rev. Gen. Electr.* **78** (1969) 17.

[32] ATTEN, P., MOREAU, R., *C. R. Hebd. Séan. Acad. Sci.* **270A** (1970) 415.

[33] LACROIX, J. C., ATTEN, P., *C. R. Hebd. Séan. Acad. Sci.* **278B** (1974) 689.

[34] ORSAY LIQ. CRYST. GROUP., *Liquid Crystals* 3, ed. Brown, G., Labes, M. M. (Gordon-Breach Sci. Publ.) 1972, pt. II, p. 711.

[35] HELFRICH, W., *J. Chem. Phys.* **51** (1969) 4092.

[36] BARNIK, M. I., BLINOV, L. M., GREBENKIN, M. F., PIKIN, S. A., CHIGRINOV, V. G., *Phys. Lett.* **51A** (1975) 175.

[37] DE JEU, W. H., GERRITSMA, C. J., VAN ZANTEN, P., GOOSSENS, W. J. A., *Phys. Lett.* **39A** (1972) 355.

[38] BARNIK, M. I., BLINOV, L. M., GREBENKIN, M. F., PIKIN, S. A., CHIGRINOV, V. G., *Zh. Eksp. Teor. Fiz.* **69** (1975) 1080 (engl. transl. : *Sov. Phys. JETP* **42** (1976) 550).

[39] MADHUSUDANA, N. V., KARAT, P. P., CHANDRASEKHAR, S., *Current Sci.* **42** (1973) 147.

[40] DUBOIS-VIOLETTE, E., DE GENNES, P. G., PARODI, O., *J. Physique* **32** (1971) 305.

[41] SMITH, I. W., GALERNE, Y., LAGERWALL, S. T., DUBOIS-VIOLETTE, E., DURAND, G., *J. Physique Colloq.* **36** (1975) C1-237.

[42] CHIGRINOV, V. G., PIKIN, S. A., *Kristallografiya* **23** (1978) 333.

[43] BELYAYEV, S. V., BLINOV, L. M., *Zh. Eksp. Teor. Fiz.* **70** (1976) 184 (Engl. transl. : *Sov. Phys. JETP* **43** (1976) 96).

[44] HELFRICH, W., *J. Chem. Phys.* **55** (1971) 839.

[45] HURAULT, J. P., *J. Chem. Phys.* **59** (1973) 2068.

[46] PIKIN, S., RYSCHENKOW, G., URBACH, W., *J. Physique* **37** (1976) 241.

[47] PIKIN, S. A., CHIGRINOV, V. G., INDENBOM, V. L., *Mol. Cryst. Liq. Cryst.* **37** (1976) 313.

[48] GOSCIANSKI, M., *Philips Res. Rep.* **30** (1975) 37.

[49] TIKHOMIROVA, N. A., GINSBERG, A. V., KIRSANOV, E. A., BOBYLEV, Ju. P., PIKIN, S. A., ADOMENAS, P. V., *Pis'ma Zh. Eksp. Teor. Fiz.* **24** (1976) 301.

[50] MATYUSHICHEV, Yu. F., KOVNATSKI, A. M., *Zh. Tekh. Fiz.* **45** (1975) 661.